Magnetic resonance imaging assessment of body composition parameters in Crohn's disease

Ghislain Labarthe, Michael Dolores, Mikael Verdalle-Cazes, Cloe Charpentier, Pauline Roullee, Jean-Nicolas Dacher, Guillaume Savoye, Céline Savoye-Collet

Version of Record: https://www.sciencedirect.com/science/article/pii/S159086582030308X
Manuscript_78e67766ff55801c329648e88fd08028

Daphnanes diterpenes from the latex of *Hura crepitans* L. and activity against human colorectal cancer cells Caco-2

Manon Trinel[a], Anne-Cécile Le Lamer[a,*], Valérie Jullian[a,b], Denis Jacquemin[c], Jérôme Graton[c], Valérie Cristofoli[a], Elise Crossay[a], May Yassine[d], Corinne Rolland[d], Nathalie Vergnolle[d], Kember Mejia[e], Billy Joel Cabanillas[b], Claire Racaud-Sultan[d,*,1], Nicolas Fabre[a,1].

[a] UMR 152 PharmaDev, Université de Toulouse, IRD, UPS, France
[b] Laboratorios de Investigación y Desarrollo, Facultad de Ciencias y Filosofía, Universidad Peruana Cayetano Heredia, Lima 15102, Peru
[c] CEISAM, Chimie et Interdisciplinarité, Synthèse, Analyse, Modélisation, Faculté des Sciences et des Techniques, Université de Nantes, France
[d] IRSD, Université de Toulouse, INSERM, INRA, ENVT, UPS, Toulouse, France
[e] Instituto de Investigaciones de la Amazonia Peruana (IIAP), Iquitos, Peru

* Claire Racaud-Sultan, INSERM Unité 1220, Institut de Recherche en Santé Digestive IRSD, CHU Purpan, Place du Dr Baylac, 31024 Toulouse cedex 3, France. Email addresss: claire.racaud@inserm.fr; Anne-Cécile Le Lamer, UMR 152 PharmaDev, Université Paul Sabatier, Faculté de Pharmacie, 35 chemin des maraichers, 31062 Toulouse, France. Email address: anne-cecile.le-lamer@univ-tlse3.fr.
[1] These authors contributed equally to the work.

KEYWORDS
Hura crepitans, daphnanes diterpenes, colorectal cancer, cytotoxicity, epithelial morphogenesis

ABSTRACT
Hura crepitans (Euphorbiaceae) is a tree from South America that produces an irritant latex used as a fish poison. A bio-guided fractionation of an ethanolic extract of the latex led to the isolation and structural identification of three known daphnane-type diterpenes (**1**-**3**) including huratoxin (**1**), together with two new analogues (**4**, **5**). Compound **1** was found to exhibit significant and selective cell growth inhibition against the colorectal cancer cell line Caco-2, with morphological modifications suggesting formations mimicking the intestinal crypt architecture. The underlying mechanism of **1** was further investigated, in comparison with 12-O-tetradecanoylphorbol-13-acetate (TPA), revealing two different mechanisms.

GRAPHICAL ABSTRACT

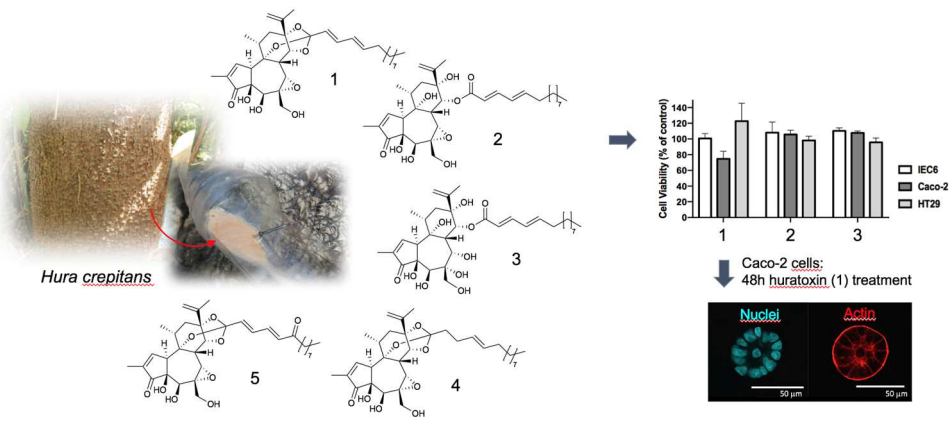

1. Introduction

Hura crepitans L. is a tall thorn-covered tree of the Euphorbiaceae family producing a milky and irritant latex, widely distributed in South America and some African and Asian countries [1]. In a previous phytochemical analysis, we identified daphnanes diterpenes and cerebrosides as the main chemical constituents of an ethanolic extract of the latex of *H. crepitans* [2]. Daphnanes diterpenes are known for their multiple biological activities [3,4], such as piscicidal [5,6], antiviral [7,8], anti-HIV [9–11], anti-cancer [7,10], as well as tumor promoting [16,17] activities. Importantly, daphnanes diterpenes could restore tissue functions such as in neurodegenerative diseases [18], notably through anti-inflammatory activities [4,19]. They are also described as activators of the serine threonine protein kinases C (PKCs) [15] that play a critical role as early signal in diverse cellular responses and are particularly downregulated in colorectal cancer. PKC are not necessarily down regulated in cancer cells but are often targets for inactivating mutations which clearly indicates a tumor suppressor activity for these ser/thr kinases [20].

Colorectal cancer is a global scourge with, according to the OMS, 1 million of new cases detected each year and 774 000 deaths. In 2018, it is the third deadliest (after lung and liver) cancers [21]. Depending on the tumor characteristics and extend of disease, the treatment of patients includes surgery, chemotherapy and targeted therapies. However, the tumor plasticity induces resistance to therapy through surviving and quiescent cancer stem cells [22], and is responsible for high mortality. Given the reversible nature of mechanisms implicated in tumor plasticity, novel therapeutic approaches aiming to restore tissue homeostasis are promising. The efficiency of these new therapies will depend on their capacities to normalize the dialog between epithelial cells and their microenvironment, locally in the intestine and at distance in metastasis. Locally, the aim of such therapies would be to get reconstruction of the intestinal crypt characterized by a polarized epithelial monolayer playing a barrier role against external environment through intercellular adhesive junctions and capable of differentiation towards absorptive and secretory lineages [23].

Therapeutic targeting of early signals such as PKCs, which coordinate adhesive and proliferative pathways in epithelial cells [24], may be of great interest to control different tumor cell subpopulations [25]. As an example, the small TPA (12-O-Tetradecanoylphorbol-13-acetate) molecule is a natural phorbol ester diterpene and a PKC activator which has been recently shown to inhibit liver transformation through the regulation of YAP (Yes-associated protein), the major effector of the Hippo signaling pathway at the crossroad of cell adhesion

and proliferation [26]. In that context, natural compounds constitute a promising source of novel anticancer agents, capable of modulating embryonic developmental proliferative pathways such as Wnt/APC/β-catenin in cancer stem cells and managing adhesive interactions with the cancer microenvironment [27].

In this paper, we describe the bio-guided fractionation of the latex of *H. crepitans* leading to the isolation and identification of three known daphnane-type diterpenes huratoxin, prohuratoxin and stelleralide J, along with two new analogs of huratoxin, namely, 2',3'-dihydrohuratoxin and 6'-oxohuratoxin. Cytotoxic assays of enriched fractions and pure compounds against the human colorectal cancer Caco-2 cell line are presented and mechanisms of action are also proposed for huratoxin in comparison with TPA.

2. Material and methods

2.1 *Plant material*

The latex of *H. crepitans* L. was collected in the area of Mazán, Maynas province, Peru, in March 2017 by Dr. Billy Joel Cabanillas. Botanical identification was carried out by Diego Garcia (Forestry engineer, IIAP, Peru) and Pr. Isabelle Fourasté (faculty of Pharmacy, Toulouse University, France). The deposition of a herbarium board (No. Hc2017-1) was made in the herbarium collection of the faculty of pharmacy of Toulouse, France.

2.2 *Analytical chemistry material*

The IR spectra were acquired on a Fourier transform spectrophotometer FRONTIER FT-IR (PerkinElmer, CT, USA). UV spectra were acquired on a Jasco J-815 UV-visible spectrophotometer (Jasco Inc, Easton, MD, USA). The optical rotation was calculated on a Jasco P-2000 polarimeter in CH_2Cl_2 (Jasco Inc, Easton, MD, USA). Circular dichroism (CD) spectra were measured in CH_2Cl_2 on a Jasco J-815 spectrophotometer (Jasco Inc, Easton, MD, USA). UHPLC/DAD/CAD/HRMS analysis were performed using an UHPLC Ultimate 3000 system (Dionex, Sunnyvale, CA, USA) equipped with an Acquity UPLC BEH C18 100Å column (150 x 2.1 mm, 1.7 µm) (Waters Corporation), a Diode Array Detector system (Dionex, Sunnyvale, CA, USA) and a Charge Aerosol Detector (Dionex, Sunnyvale, CA, USA) for relative quantitative analysis. High resolution APCIMS spectra were acquired on a LTQ-Orbitrap mass spectrometer (Thermo Fisher Scientific, Bremen, Germany). Chromeleon Xpress 6.8 (Dionex) and Xcalibur 3.0 (Thermo Fischer Scientific) softwares were used for data acquisition and analysis. Analytical LC/UV analyses were performed using a HITACHI

LaChrom ULTRA UHPLC chain equipped with a diode array detector system (VWR, PA, USA) and an Acquity UPLC BEH C18 100Å column (150 x 2.1 mm, 1.7 µm) (Waters Corporation). Semi-preparative HPLC was performed on a HITACHI LaChrom LC system (VWR, PA, USA) consisting in a quaternary LaChrom L-7100 pump and a LaChrom L-7455 photodiode array detector using a Phenomenex Luna column C18 100Å (10 x 250 mm, 5 µm) (Phenomenex Inc, CA, USA). Preparative HPLC was performed on a Waters 4000 system (Millipore) equipped with a Jasco UV-975 photodiode array detector using a SunFire Prep Silica column C18 100Å (19 x 150 mm, 5 µm) (Waters Corporation). MPLC were performed using a BUCHI system composed by 2 C-605 pumps controlled by a C-615 pump manager, in borosilicated glass columns (Buchi, Flawil, Switzerland) conditioned by silica gel Kieselgel 60® (Macherey-Nagel, Duren, Germany) previously dried at 100 °C. NMR spectra were acquired on a Bruker AVANCE 300 and a Bruker AVANCE 500 spectrometer equipped with a 5 mm TCI CryoProbe (Bruker, Fällanden, Switzerland) using TMS as reference. Column chromatographies were performed using silica gel Kieselgel 60 (Macherey-Nagel, 15-40 µm) and previously dried at 100 °C before use.

2.3 *Extraction and isolation of mono-esterified daphnanes*

2.3.1 *Extraction of the latex of H. crepitans*

The lyophilized latex of *H. crepitans* (382 g) obtained from 2.4 L of latex was extracted by 2 successive macerations with 3.8 L of 96% EtOH during 24 h at room temperature. After filtration, the residue was extracted twice with 2 x 3.8 L of CH_2Cl_2 during 1 h under reflux. The solvents of both extractions were combined and concentrated under reduced pressure to give 34 g of crude extract.

2.3.2 *Fractionation of the crude extract*

6 g of the crude extract of the latex of *H. crepitans* was partitioned by medium-pressure liquid chromatography (MPLC) on silica gel using *n*-heptane (650 mL), CH_2Cl_2 (2 L), EtOAc (650 mL), methanol (2 L) and isopropanol (650 mL). This fractionation was repeated five times on 6 g of crude extract. The fractions were combined to give nine fractions (F_1-F_9). Each fraction was analyzed by UHPLC/DAD/CAD/HRMS according to Trinel et al. [2]. F_7 (2 g) was highly concentrated in cerebrosides while F_3 (3.4 g) and F_5 (5.93 g) were both enriched in mono- and di-esterified daphnanes. Separation of the daphnanes from fraction F_3 was carried out by MPLC with CH_2Cl_2 (1.5 L), CH_2Cl_2/EtOAc (1 L, 4:1, v/v), EtOAc (1 L) and MeOH (0.5 L) to afford 3 sub-fractions $F_{3\text{-}1}$-$F_{3\text{-}3}$, $F_{3\text{-}2}$ (2.28 g) and $F_{3\text{-}3}$ (0.82 g) being enriched in di- and mono-esterified daphnanes respectively. UHPLC/DAD/CAD/HRMS analysis of the mono-esterified

daphnanes was performed using an optimized gradient consisting in milliQ water (solvent A) and MeCN (solvent B) each containing 0.1% of formic acid. The gradient started from 70% B for 2 min, linearly increased to 100% B from 2 to 17 min and remained constant for 11 min à 100% B, before it decreased to 70% B in 0.5 min and remained at initial conditions for 1.5 min.

2.3.3 *Isolation of mono-esterified daphnanes*

$F_{3\text{-}3}$ (0.82 g) was chromatographed on a silica gel column using a cyclohexane/EtOAC gradient (from 8:2 to 0:10, v/v) to give 8 sub-fractions ($F_{3\text{-}3.1}$-$F_{3\text{-}3.8}$). $F_{3\text{-}3.5}$ was separated by semi-preparative HPLC using a H_2O/MeCN (each containing 0.1% of formic acid) linear gradient (3 mL/min) from 15% MeCN to 100% MeCN to provide compounds **1** (Huratoxin, 18.1 mg) and **4** (2',3'-dihydrohuratoxin, 2.7 mg). Fraction $F_{3\text{-}3.7}$ was purified by semi-preparative HPLC (3 mL/min) with a linear gradient from 20% MeCN to 100% MeCN to afford 3 subfractions ($F_{3\text{-}3.7\text{-}1}$-$F_{3\text{-}3.7\text{-}3}$). Compound **2** (Prohuratoxin, 1.8 mg) was isolated from $F_{3\text{-}3.7\text{-}2}$ by semi-preparative HPLC following the same method as for $F_{3\text{-}3.7}$.

Fraction F_5 (5.93 g) was fractionated twice by MPLC using a solvent gradient of increasing polarity from cyclohexane to EtOAc (500 mL), affording 7 fractions ($F_{5\text{-}1}$-$F_{5\text{-}7}$). $F_{5\text{-}5}$ (1.66 g) was chromatographed by preparative HPLC (flow rate: 20.5 mL/min) with a linear gradient starting from 60% MeCN to 100% in 15 min to obtain 19 subfractions ($F_{5\text{-}5.1}$-$F_{5\text{-}5.19}$). Subfraction $F_{5\text{-}5.3}$ was subjected to semi-preparative HPLC (3 mL/min) using an isocratic solvent system of 85% MeCN during 30 min to yield compound **3** (Stelleralide J, 7.4 mg). Compound **5** (6'-oxohuratoxin, 2.1 mg) was obtained from the $F_{5\text{-}5.8}$ subfraction by semi-preparative HPLC using the same gradient as the one used for the obtention of compounds **1** and **4**.

Huratoxin **1**: colorless oil, $[\alpha]_{25}^{D}$ +39.6 (c 1, CH_2Cl_2); IR υ_{max} 3467, 2926, 2855, 1696, 1633, 1276 cm^{-1}; ^1H and ^{13}C NMR data ($CDCl_3$, 500 MHz), see Table 1; HRAPCIMS *m/z* 585.3406 $[M+H]^+$ Δppm = -2.7 (calcd for $C_{34}H_{49}O_8^+$, 585.3422).

Prohuratoxin **2**: colorless oil, $[\alpha]_{25}^{D}$ +18.4 (c 1, CH_2Cl_2); IR υ_{max} 3447, 2925, 2854, 1701, 1633, 1300 cm^{-1}; ^1H and ^{13}C NMR data ($CDCl_3$, 500 MHz), see Table 1; HRAPCIMS *m/z* 603.3508 $[M+H]^+$ Δppm = -3.3 (calcd for $C_{34}H_{51}O_9^+$, 603.3528).

Stelleralide J **3**: colorless oil, $[\alpha]_{25}^{D}$ +27.6 (c 1, CH_2Cl_2); IR υ_{max} 3467, 2926, 2855, 1696, 1633, 1276 cm^{-1}; ^1H and ^{13}C NMR data ($CDCl_3$, 500 MHz), see Table 1; HRAPCIMS *m/z* 619.3498 $[M–H]^–$ Δppm = 3.1 (calcd for $C_{34}H_{51}O_{10}^–$, 619.3479).

2',3'-dihydrohuratoxin **4**: colorless oil, $[\alpha]_{25}^{D}$ +44.8 (c 1, CH_2Cl_2); IR υ_{max} 3467, 2926, 2855, 1693, 1633, 1276 cm^{-1}; ^{1}H and ^{13}C NMR data ($CDCl_3$, 500 MHz), see Table 1; HRAPCIMS *m/z* 587.3573 $[M+H]^+$ Δppm = -1.9 (calcd for $C_{34}H_{51}O_8^+$, 587.3584).

6'-oxohuratoxin **5**: colorless oil, $[\alpha]_{25}^{D}$ +25.8 (c 1, CH_2Cl_2); IR υ_{max} 3467, 2926, 2855, 1699, 1633, 1276 cm^{-1}; ^{1}H and ^{13}C NMR data ($CDCl_3$, 500 MHz), see Table 1; HRAPCIMS *m/z* 599.3204 $[M+H]^+$ Δppm = -2.7 (calcd for $C_{34}H_{47}O_9^+$, 599.3220).

2.4 *Computational analysis*

Calculated Electronic Circular Dichroism (ECD) spectra were also modelled by first principles. These DFT and TD-DFT calculations were performed using the Gaussian16 program [25]. The calculations consisted in three successive steps. First, we optimized the ground-state geometries of the anticipated enantiomers at the B3LYP/6-311G(d,p) level [29]. These calculations used the so-called *tight* optimization threshold, a refined DFT integration grid (the *ultrafine* grid was selected), and a tightened SCF convergence thresholds (10^{-10} au). The bulk solvent effects (here CH_2Cl_2) were accounted for using the Polarizable Continuum Model (PCM) [30]; selecting the Gaussian16 defaults to build the cavity. In a second stage, the vibrational frequencies have been evaluated at the same level of theory to confirm the nature of the obtained structures (absence of imaginary frequency). In a third step, TD-DFT calculations were performed at the CAM-B3LYP/6-311+G(2d,p) level in order to model the ECD spectra of the envisaged enantiomers. These calculations included the 25 lowest single excited-states and used the PCM model in its linear-response non-equilibrium form, which is suited for modeling absorption and ECD spectra [31]. The presented spectra have been convoluted, from the individual vertical contributions, using a Gaussian with of half-width at half-maximum of 0.33 eV.

2.5 *Cell culture*

The human colon adenocarcinoma cell line Caco-2 (HTB-37) was purchased from the American Type Culture Collection (ATCC, Manassas, VA, USA). Two other cell lines from ATCC were used as comparison in cytotoxic assays: the normal rat intestinal epithelial cell line IEC6 (CRL-1592) and the human colon adenocarcinoma cell line HT29 (HTB-38). Of note, both Caco-2 and HT29 cell lines harbor APC mutation, the most frequent mutation in colorectal cancer, responsible for hyperproliferation through the dysregulated Wnt/APC/β catenin pathway. All cell lines were cultured in DMEM + GlutaMAX medium (Corning, New York, NY, USA) supplemented with 10% fetal bovine serum (Thermo Fisher Scientific,

Waltham, MA, USA), 100 units/mL penicillin and 100 units/mL streptomycin (Thermo Fisher Scientific). For Caco-2 cells, 1% of non-essential amino acids was added to the medium. Cells were incubated at 37°C in a 95% relative humidity atmosphere with 5% CO_2. Medium was changed every 48 h and passage was performed every week before confluence.

2.6 *Cell treatment and viability assay*

Cells were seeded at 8 x 10^4 cells/100 µL in 96-well plates (Falcon, Corning Life Sciences, Amsterdam, The Netherlands) and cultured for 48 h before treatment with varying concentrations of natural extracts or compounds. Initial solution of extracts or compounds was prepared in dimethyl sulfoxide (DMSO) at 10 mg/mL and then successive dilutions (from 1/1000 to 1/100 000) in fresh culture medium were incubated with cells. Controls assays were realized with diluted DMSO (final concentration from 0.1% to 0.001%) in culture medium. After 48 h of treatment, cell viability was determined by adding 20 µL of the Aqueous One Solution Cell Proliferation Assay (MTS, Promega) to each well for 3 h. The colorimetric assay was then evaluated by the measurement of absorbance at 490 nm using a microplate reader (Varioskan Flash, Thermo Fisher Scientific). Assays were performed in triplicate.

2.7 *Fluorescence analysis and imaging*

Immunolabeling: Caco-2 cells were seeded at 4 x 10^4 cells/40 µL in 15 well IBIDI plates (Biovalley, Nanterre, France) and treated as described above. At 24 h and 48 h post-treatment, cells were fixed with formaldehyde solution (3.7%, Electron Microscopy Sciences) during 20 min at room temperature before 3 washes with phosphate buffer saline (PBS) and then conservation at 4°C. A permeabilization step was realized by 3 x 10 min incubation with PBS supplemented with Triton X100 0.5% and BSA 1%. Then primary antibody (anti-Ki67 Ab16667 1/50 or anti-caspase 3 active Ab13847 1/200, Abcam, Paris, France) was added overnight at 4°C. Then the secondary antibody (anti-rabbit Alexa Fluor 488-conjugated 1/1000, Invitrogen Molecular Probes, Thermo Fisher Scientific, Illkirch, France) was added for 1 h followed after 3 washes by incubation with rhodamine phalloidin (5 units/mL, R415 Invitrogen) for 30 min, at room temperature. Finally, VECTASHIELD with DAPI (Eurobio, Montpellier, France) was added and samples were conserved at 4°C until microscopic analysis.

Premo-FUCCI cell cycle sensor (Molecular probes, Life technologies): Caco-2 cells were seeded at 4 x 10^4 cells/100 µL in 96-well plates and incubated with 50 viral particles per cell

(PPC 50) containing Premo-geminin GFP (S/G2/M reagent) and Premo-Cdt1 RFP (G1 reagent). 24 h after, transfection enhancer (1/1000, Invitrogen) was added to the culture medium. On the next day, cells were treated with 1 µg/mL of huratoxin or TPA, or DMSO as control. Cell imaging was performed from 24 h to 96 h after treatment.

Bright field and GFP/RFP images were acquired with Apotome microscope (Zeiss Axio-observer, HXP120) and immunofluorescence was visualized with confocal laser scanning using Zeiss LSM710 (Leica Microsystems, Heerbrugg, Germany). Images were then analyzed with the Image J software.

2.8 *Western Blot*

Caco-2 cells were seeded at 64 x 10^4 cells/1000 µL in 12-well plate (Falcon) and treated as described above. At 48h post-treatment and after two washes with PBS plus Ca^{2+}/Mg^{2+}, cells were lysed in buffer containing 50 mM Tris-HCl pH 7.5, 150 mM NaCl, 0.1% Triton X-100, 1 mM EDTA supplemented with proteases inhibitor (1/25, cOmplete™ Mini, EDTA-free, Roche, Sigma-Aldrich, L'Isle d'Abeau Chesnes, France) and phosphatases inhibitor (1/100, Phosphatase Inhibitor cocktail 2, Sigma-Aldrich). After 20 min of incubation on ice and scraping, samples were centrifuged at 12 000 g for 15 min at 4°C. Sample protein concentration in the supernatant (Triton X-100 soluble fraction) was measured and then Laemmli sample buffer 5x was added before conservation at -20°C.

After boiling for 10 min, proteins were resolved on 10% acrylamide precast gel (Mini-PROTEAN TGX, Bio-Rad, Marnes-la-Coquette, France) and transferred to nitrocellulose membrane (Hybond C-super, Merck Millipore, Molsheim, France). The membrane was blocked for 1 h at room temperature in Tris-buffer saline (TBS) containing 0.5% fat-free milk and 1% bovine serum albumin (BSA, Sigma). Then membrane was probed overnight at 4°C with the appropriate antibody in TBS-milk-BSA supplemented with 0.05% Tween. Primary antibodies were from Cell Signaling Technology (phospho-p44/42 MAPK #4370; 44/42 MAPK #9102; phospho-Akt (Ser473) #4060; Akt #4685; phospho-YAP (Ser127) #13008; YAP #1407), Millipore (phospho-GSK3β (Ser9) #04-1075), BD Biosciences (GSK3β #610202), Abcam (Actin #Ab 1801). After incubation for 1 h at room temperature with secondary antibody coupled to horseradish peroxidase, detection was achieved using a chemiluminescent substrate (Amersham ECL Prime detection reagent, Sigma-Aldrich) and visualized on ChemiDoc (Bio-Rad).

2.9 *Reverse transcriptase-polymerase chain reaction (RT-PCR)*

Caco-2 cells were seeded at 64 x 10^4 cells/1000 µL in 12-well plate (Falcon) and 48 h post-treatment were washed with PBS before addition of TRisol Reagent (Thermo Fisher Scientific) and RNA extraction with Direct-zol RNA kit (Ozyme, Saint-Cyr-L'Ecole, France), according to manufacturer's instructions, including a 15 min DNAse (RNAse free) treatment at room temperature. Nucleic acid quantification and purity were assessed by the absorbance A_{260} and the ratio A_{260}/A_{280}, respectively (Nanodrop 2000, Thermo Fisher Scientific). Three µg RNA were reverse-transcribed in 14 µl reaction volume using the Maxima first strand kit and following the manufacturer's instructions (Fermentas, Thermo Fisher Scientific). Quantitative PCR was prepared with LightCycler 480 DNA SYBR Green I Master reaction mix (Roche, Mannheim, Germany) and 45 ng cDNA was used as template for amplification (40 cycles, 60°C) using 0.6 µM specific primers: ITGA2 (GTGGCTTTCCTGAGAACCGA/GATCAAGCCGAGGCTCATGT, NM_002203), MUC2 (ACTCCAACATCTCCGTGTCC/AGCCACACTTGTCTGCAGTG, NM_002457). The run was performed in two technical replicates on a LightCycler 480 Instrument (Roche). All primers used have PCR efficiency >90%. *Hprt* and *Gapdh* were used as reference genes. The delta Ct was calculated (Microsoft Excel software) from the means of reference gene and target gene duplicates. DdCt was used to perform comparisons between different treatments.

2.10 *Statistical analysis*

Anova tests were used for experiments analysis. *P* values <0.05 were considered to be significant and the correction used for multiple comparisons is indicated on the figures.

3. Results and Discussion

3.1 *Bio-guided fractionation of the latex of H. crepitans.*

The *in vitro* cytotoxicity of the crude extract of the latex of *H. crepitans* was determined using two human colorectal cancer cell lines Caco-2 and HT29, and a rat intestinal cell line IEC6. As shown in **Fig. 1A**, depending on cell line and concentration of crude extract, the number of viable cells was significantly decreased (-34.33% ± 2.52 at 1 µg/mL, and -23.00% ± 4.36 at 10 µg/mL) only for Caco-2 cells, thus revealing a valuable selectivity towards the human colorectal cancer cells Caco-2 from a concentration of 1 µg/mL.

As shown in **Fig. 1B**, morphological modifications were observed under the treatment with crude extract. Spreading (IEC6 cells), polarization (HT29 cells), and clustering (Caco-2 cells) were observed suggesting a potential link between morphological changes and cytotoxicity induced by the crude extract of the *H. crepitans* latex. We underline that no cell death was observed suggesting that the decrease of Caco-2 cells number under treatment was due to a cytostatic effect.

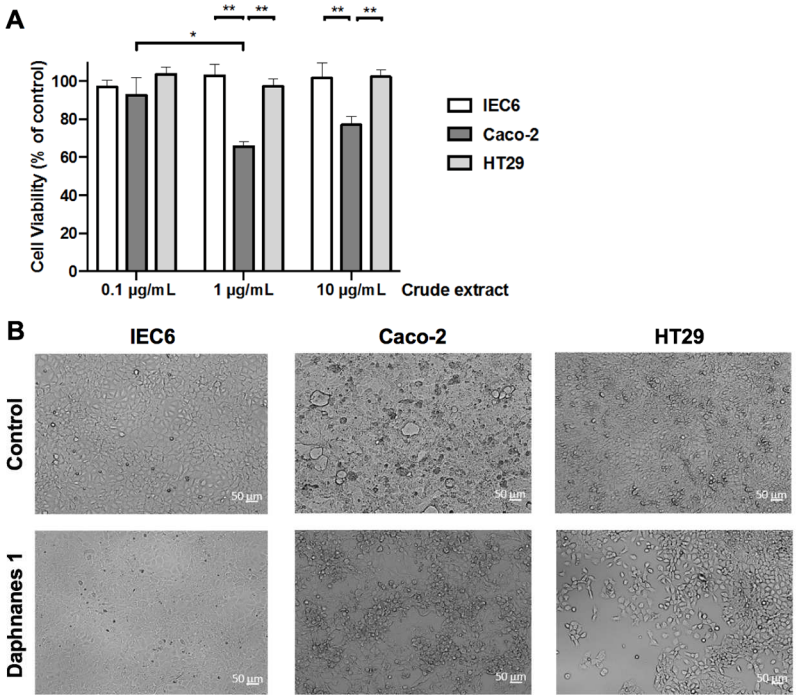

Figure 1. (**A**) Cytotoxicity of the crude extract of *H. crepitans* latex. IEC6 (normal intestinal cell line), Caco-2 and HT29 (colon cancer cell lines) cells were incubated with different concentrations of the crude extract of the latex of *H. crepitans* or DMSO as control. At 48 h, a MTS assay was performed to measure surviving cells. Data are mean ± S.D. from 3 independent experiments. Two-way Anova (Tukey's multiple comparisons test): *p<0.05, **p<0.01. (**B**) Morphological changes induced by the crude extract of *H. crepitans* latex. IEC6, Caco-2 and HT29 cells were incubated with 10 µg/mL crude extract of *H. crepitans* latex or DMSO and microscopic observations were performed at 48 h post-treatment. Bar = 50 µm.

The above biological results prompted a further study to determine which kind of compounds was responsible for this selective cytotoxicity. Our previous work highlighted that the latex of *H. crepitans* was composed of three major types of compounds that could be divided in mono-esterified daphnanes, di-esterified daphnanes and cerebrosides [2]. Complementary relative quantitative analysis with a Charged Aerosol Detector (CAD) confirmed that daphnanes and cerebrosides were the main compounds of the crude extract (see the Supporting Information, SI). Mono-esterified and di-esterified daphnanes represented around 25 and 40% of the mixture respectively, while cerebrosides accounted for around 30%. The crude extract was thus partitioned by repeated reverse-phase MPLC to afford fractions enriched in mono-esterified daphnanes, di-esterified daphnanes or cerebrosides.

Results of incubation of the corresponding enriched fractions at 10 µg/mL with the three cell lines are presented in **Fig. 2A**. Di-esterified daphnanes and cerebrosides fractions did not exert any statistically significant activity against the three cell lines. Only mono-esterified daphnanes clearly reproduced the cytostatic effect previously obtained with the crude extract on Caco-2 cells, indicating that this effect is mostly carried by one or several mono-esterified daphnanes. Our results were in agreement with previous studies that revealed that mono-esterified daphnanes exhibited *in vitro* moderated to significant cell growth inhibition against a large panel of cancer cell lines, including colorectal cancer SW480 and HCT116 cell lines [9,12] whereas di-esterified daphnanes were less potent [32,33]. In addition, the absence of cerebrosides' effect could be explained by the fact that they are source of both ceramides and sphingosines, respectively modulators and enhancers of the proliferation of intestinal epithelial cells, including Caco-2 cells [34–36]. As shown for the crude extract, mono-esterified daphnanes triggered clustering of Caco-2 cells and polarization of HT29 cells, with no sign of cell death (**Fig. 2B**). Thus, to assess the *in vitro* activity of pure mono-esterified daphnanes on Caco-2 cells, their isolation and identification were undertaken.

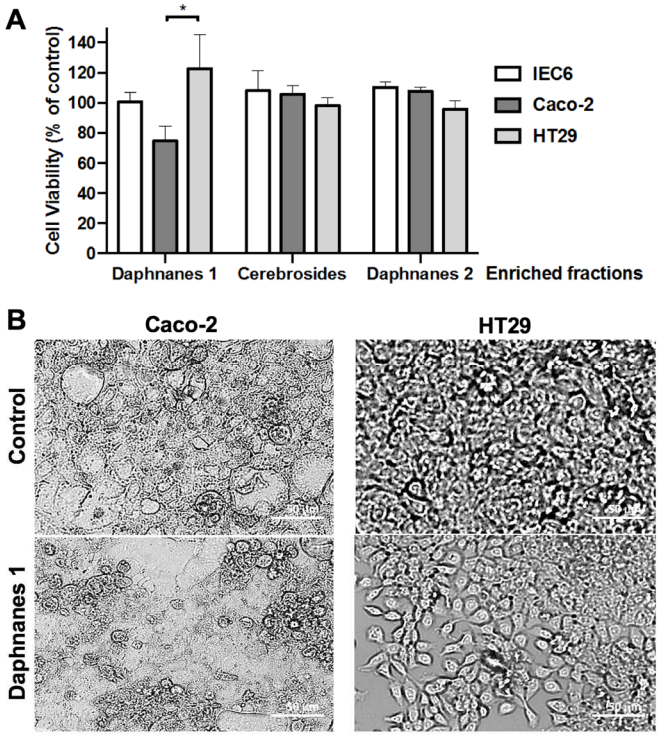

Figure 2. (**A**) Cytotoxicity of daphnanes and cerebrosides of the *H. crepitans* latex. IEC6 (normal intestinal cell line), Caco-2 and HT29 (colon cancer cell lines) cells were incubated with 10 µg/mL of mono-esterified daphnanes (Daphnanes 1), di-esterified daphnanes (Daphnanes 2) or cerebrosides. DMSO was used as control. At 48 h, a MTS assay was performed to measure surviving cells. Data are mean ± S.D. from 3 independent experiments. Two-way Anova (Tukey's multiple comparisons test): *$p<0.05$. (**B**) Morphological changes induced by mono-esterified daphnanes of the latex of *H. crepitans*. Caco-2 and HT29 cells were incubated with 10 µg/mL of mono-esterified daphnanes (Daphnanes 1) or DMSO (Control) and microscopic observations were performed at 48 h post-treatment. Bar = 50 µm.

3.2 *Isolation and structure elucidation of mono-esterified daphnanes from the latex of H. crepitans.*

Dereplication and relative quantitative analysis of the mono-esterified daphnanes by UHPLC-DAD-CAD-HRMS (see the SI) revealed that huratoxin and its isomers represented the major mono-esterified daphnanes (> 60%), along with isomers of prohuratoxin (around 20%), 5-deoxy-6,7-deepoxy-6,7-didehydrohuratoxin (around 6%), stelleralide J and deoxyhuratoxin (around 1.5% each). Moreover, minor unidentified mono-esterified daphnanes were highlighted. Separation using combination of normal and reversed-phase column chromatographies, MPLC, and semi-preparative HPLC afforded five compounds (**1**-**5**), including two new daphnanes (**4**,**5**) (**Fig. 3**).

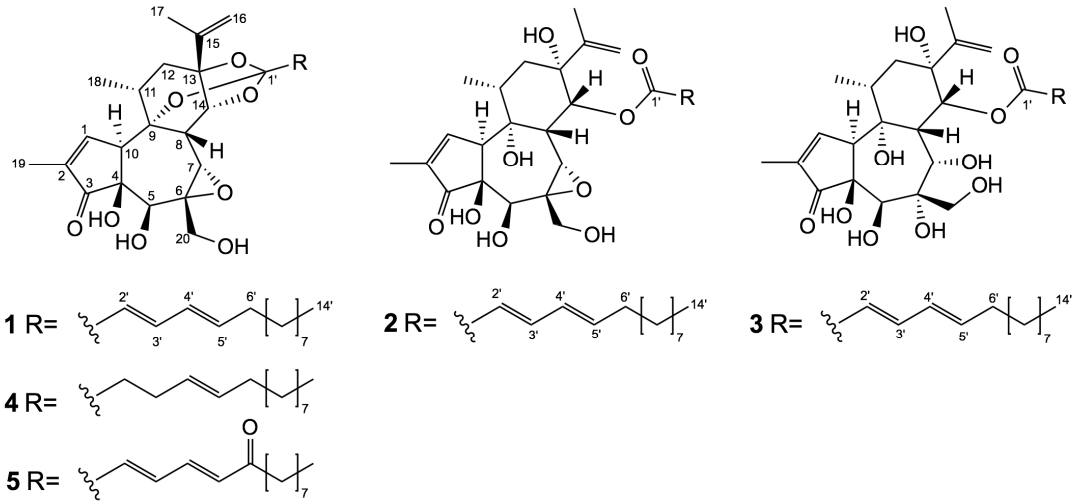

Figure 3. Structure of mono-esterified daphnanes isolated from the latex of *Hura crepitans*. Huratoxin (**1**), prohuratoxin (**2**) and stelleralide J (**3**), 2',3'-dihydrohuratoxin (**4**) and 6'-oxohuratoxin (**5**).

The three dereplicated huratoxin (**1**) [37,38], prohuratoxin (**2**) [17]**,** and stelleralide J (**3**) [5] were isolated and identified by comparison of their spectroscopic data with previously published works. The detailed ^{1}H and ^{13}C NMR data reported in **Table 1** indicated that compound **1** was a daphnane orthoester with a characteristic resonance at δ_C 116.5 for C-1', while compounds **2** and **3** were daphnanes esters with a chemical shift for C-1' at δ_C 167.5 and 167.7, respectively. A close examination of published ^{13}C NMR data of huratoxin (**1**) [37–40] compared to our 2D NMR experiments (HSQC, HMBC) revealed some errors and led us to revise the ^{13}C NMR chemical shifts of C-7, C-10, C-17, C-18, C-2', C-3', C-4' and C-5', as proposed in **Table 1**. Indeed, the HSQC spectrum of huratoxin (**1**) clearly showed that the carbons at δ_C 48.2 and 64.2 were correlated to H-10 (δ_H 3.79,) and H-7 (δ_H 3.45), respectively. Therefore, the resonance at δ_C 64.2 was assigned to the oxygenated C-7 and the one at δ_C 48.2 to C-10. Regarding the three methyl groups of the daphnane orthoester moiety, Wang et al. previously corrected the assignments of C-18 and C-19 [40]. The present HSQC experiment confirmed the revision proposed for C-19, but the correlations between H-18 (δ_H 1.18) and the carbon signal at δ_C 20.4, and between H-17 (δ_H 1.80) and the carbon signal at δ_C 19.0 indicated that the signal at δ_C 20.4 should be assigned to C-18 and not to C-17. These assignments were corroborated by the key HMBC correlations depicted in **Fig. 4**. In addition, on the basis of HSQC, HMBC, and COSY correlations, the assignment of the four conjugated olefinic carbons (C-2' to C-5') of the orthoesterified chain was unambiguously established.

Compound **4** was isolated as a colorless oil. Its molecular formula was established as $C_{34}H_{50}O_8$ by positive HRAPCIMS (*m/z* 587.3573, $[M+H]^+$), which differed from huratoxin **1** by two additional hydrogen atoms. The MS/MS spectrum revealed the presence of a diagnostic fragment ion at *m/z* 361, consistent with a daphnane-type diterpene similar to **1** [2]. Moreover, the neutral loss of 226 Da (instead of 224 for **1**) resulting from the cleavage of the side chain suggested that the aliphatic chain of compound **4** possessed only one double bond. The IR spectrum showed two bands at 1633 and 1696 cm^{-1} corresponding to a double bond and an α,β-unsaturated ketone, respectively. A band at 3467 cm^{-1} indicated the presence of hydroxyl groups. ^1H and ^{13}C NMR data (**Table 1**) of compound **4**, as well as 2D NMR spectra, exhibited general features similar to those of huratoxin **1**, indicating they both had a daphnane skeleton with the same orthoester substitution characterized by a low-field quaternary carbon resonance at δ_C 119.1 (C-1') (**Fig. 4**). The notable differences concerned the signals belonging to the orthoester side chain, particularly the presence of only two olefinic methine signals (δ_H/δ_C 5.44/129.2 and δ_H/δ_C 5.44/130.8), along with two additional methylenes (δ_H/δ_C 2.01/34.9 and δ_H/δ_C 2.29/26.8). In the HMBC spectrum, the methylenic protons at δ_H 2.01 (H-2') showed correlations with C-1' (δ_C 119.1) and the carbons at δ_C 26.8 (C-3') and 129.2 (C-4'), suggesting an orthoester moiety with a double bond located between C-4' and C-5'. This was further supported by other HMBC and COSY correlations as depicted in **Figure 4**. Regarding its configuration, overlapping signals arising from H-4' and H-5' (δ_H 5.44, m, 2H) in the ^1H NMR spectrum prevented coupling constant determination. However, according to Gunstone et al. [41], the deshielded resonance of the allylic carbon C-6' at δ_C 32.7 was characteristic of a *trans* double bond. On the basis of these aforementioned data, compound **4** was thus identified as 2',3'-dihydrohuratoxin (**Fig. 3**).

Table I. ^{1}H- and ^{13}C-NMR ($CDCl_3$) data (δ in ppm) for the daphnane-type orthoesters huratoxin (**1**), 2',3'-dihydrohuratoxin (**4**) and 6'-oxohuratoxin (**5**) and daphnane-type esters prohuratoxin (**2**), and stelleralide J (**3**).

Position	**1**		**2**		**3**		**4**		**5**	
	δ_H (*J* in Hz)	δ_C	δ_H (*J* en Hz)	δ_C	δ_H (*J* en Hz)	δ_C	δ_H (*J* en Hz)	δ_C	δ_H (*J* en Hz)	δ_C
1	7.63 m	161.3	7.66 m	162.5	7.68 m	161.3	7.60 m	161.4	7.62 m	160.8
2	-	136.7	-	134.8	-	135.0	-	136.7	-	137.0
3	-	209.9	-	209.6	-	209.3	-	209.9	-	209.7
4	-	72.3	-	72.3	-	74.8	-	72.2	-	72.2
5	4.25 s	72.0	4.24 s	71.2	4.16 s	71.3	4.25 s	72.1	4.27 s	72.0
6	-	60.4	-	61.8	-	78.1	-	60.4	-	60.5
7	3.45 s	64.2	3.17 s	63.7	4.49 m	81.8	3.43 s	64.4	3.46 s	64.1
8	2.94 d (2.6)	36.7	3.66 d (2.4)	39.2	3.39 d (2.6)	41.3	2.90 d (2.5)	36.8	2.98 d (2.6)	36.8
9	-	79.6	-	76.3	-	77.2	-	78.8	-	80.1
10	3.79 m	48.2	3.86 m	49.9	3.66 m	53.1	3.74 m	48.2	3.81 m	48.1
11	2.48 m	34.9	2.10 m	37.6	2.26 m	36.6	2.45 m	34.8	2.51 m	34.9
12a	1.68 d (14.4)	36.5	1.79 m	37.8	1.80 m	37.5	1.64 d (14.4)	36.5	1.71 d (14.3)	34.9
12b	2.23 dd (8.6, 14.4)		1.89 m		1.93 m		2.21 dd (8.8, 14.4)		2.26 dd (8.8, 14.4)	
13	-	84.4	-	74.1	-	74.3	-	84.2	-	84.9
14	4.42 d (2.6)	82.0	5.67 m	77.9	5.65 m	79.2	4.37 d (2.5)	81.8	4.46 d (2.6)	82.1
15	-	146.1	-	145.8	-	145.1	-	146.2	-	145.7
16a	4.90 m	111.3	5.08 s	114.1	5.08 d (1.3)	114.3	4.90 m	111.3	4.93 m	111.7
16b	5.02 s		5.13 s		5.19 s		5.01 s		5.02 s	
17	1.80 br s	19.0	1.89 m	19,0	1.88 m	19.0	1.77 br s	19.1	1.79 br s	19.0
18	1.18 d (7.2)	20.4	1.06 d (6.7)	18.2	1.04 d (6.6)	17.3	1.16 d (7.1)	20.3	1.19 d (7.1)	20.4
19	1.81 d (1.4)	10.0	1.80 m	9.9	1.81 m	9.8	1.80 m	10.0	1.81 m	10.0
20a	3.78 d (12.4)	65.1	3.74 d (12.4)	65.2	3.94 d (11.6)	68.2	3.76 d (12.5)	65.3	3.78 d (12.6)	65.1
20b	3.86 d (12.4)		3.84 d (12.4)		4.06 d (11.6)		3.88 d (12.5)		3.90 d (12.6)	
1'	-	116.5	-	167.5	-	167.7	-	119.1	-	115.6
2'	5.70 d (15.5)	122.8	5.9 d (15.3)	117.7	5.86 d (15.3)	118.0	2.01 m	34.9	6.21 d (15.4)	133.5
3'	6.70 dd (10.7, 15.5)	134.8	7.33 dd (10.1, 15.3)	147.4	7.32 dd (10.1, 15.3)	147.1	2.29 m	26.8	6.82 dd (11.1, 15.4)	132.2
4'	6.05 dd (10.7, 15.2)	128.8	6.20 m	128.2	6.20 m	128.2	5.44 m	129.2	7.15 dd (11.1, 15.5)	140.1
5'	5.84 dt (15.2, 6.9)	139.0	6.20 m	146.8	6.20 m	146.6	5.44 m	130.8	6.28 d (15.5)	132.6
6'	2.08 m	32.7	2.18 m	33.1	2.19 m	33.1	1.97 m	32.7	-	200.7
7'	1.37 m		1.43 m	28.7	1.43 m	28.7			2.55 t (7.3)	40.9
8'									1.63 m	24.4
9'		29.1 - 29.6		29.2-29.5		29.2-29.6		29.2-29.7		29.0
10'	1.24-1.31 m 12H		1.24-1.32 m 12H		1.26-1.31 m 12H		1.26-1.30 m 14H			29.2 - 29.5
11'									1.24 - 1.31 m 10H	
12'		31.9		31.9		31.9		32,0		31.9
13'		22.7		22.7		22.7		22.7		22.7
14'	0.88 t (6.9)	14.1	0.88 t (6.9)	14.2	0.88 t (6.9)	14.2	0.88 t (6.9)	14.2	0.88 t (6.9)	14.1
OH-4	3.73 s	-	3.52 s	-	3.36 s	-	3.57 s	-		-
OH-5	4.09 s	-		-	3.36 s	-	4.01 d (2.6)	-		-
OH-9	-	-	-	-	3.70 s	-	-	-	-	-
OH		-		-	4.49 m	-		-		-

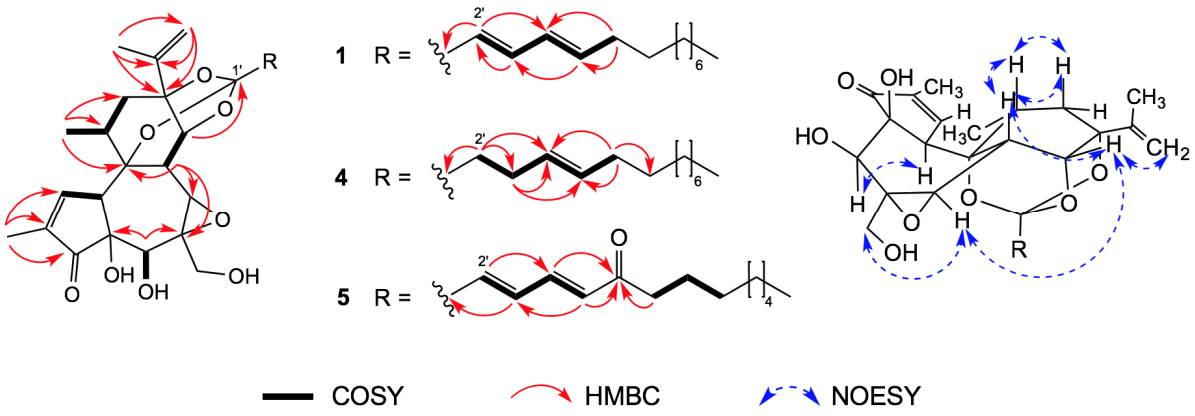

Figure 4. Key COSY, HMBC (H→C) and NOESY correlations for compounds **1**, **4** and **5**

Compound **5** was isolated as a colorless oil. Its molecular formula was established as $C_{34}H_{46}O_9$ by positive HRAPCIMS (*m/z* 599.3204, $[M+H]^+$), with 14 mass units more than huratoxin **1**. Using the same approach as for compound **4**, the diagnostic fragment ion at *m/z* 361 in the MS/MS spectrum and the NMR key signal at δ_C 115.6 in the ^{13}C spectrum were indicative of a daphnane-type orthoester. The IR spectrum showed the same bands as in compound **4**, with a broader carbonyl band at 1699 cm^{-1}. 1D and 2D NMR data (**Table 1**) were reminiscent of those of huratoxin **1**, except for the chemical shifts of four olefinic methine signals, the presence of a quaternary carbon signal at δ_C 200.7 typical of a ketone, and the disappearance of a CH_2 signal at δ_C 32.7. Analysis of COSY cross peaks revealed the presence of two spin systems CH-2'/CH-3'/CH-4'/CH-5' and CH_2-7'/CH_2-8'. Moreover, in the HMBC spectrum H-5', H-6' and H_2-7' correlated with C-6', which connected the above-mentioned spin systems together. These observations, combined with HMBC correlations from H-14 and H-3' to C-1', secured the orthoester moiety with a ketone function at C-6' (**Fig**. **4**). Compound **5** was therefore elucidated as 6'-oxo-huratoxin.

Furthermore, NOESY correlations for compounds **4** and **5** in the daphnane orthoester core were similar to those of huratoxin **1**, allowing the determination of their relative configuration (**Fig. 4**). Their absolute configuration was subsequently assigned by comparing their experimental electronical circular dichroism (ECD) spectra (**Fig. 5**) with calculated ECD spectra (**Fig. 6**).

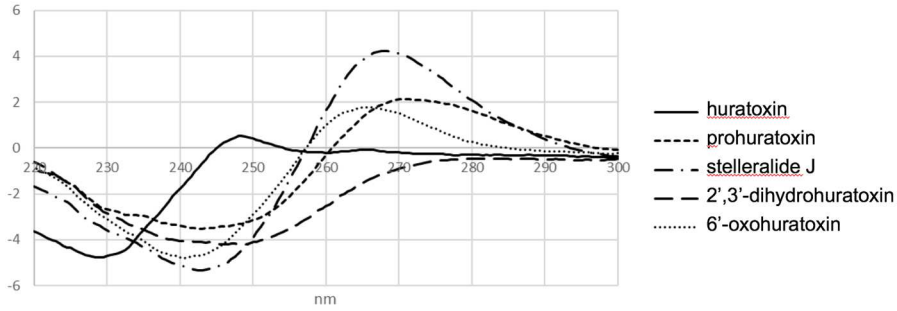

Figure 5. Experimental ECD spectra of compounds **1**-**5** in CH_2Cl_2.

First to assess the quality of the level of theory selected for the modeling studies, we have computed the ECD spectrum of huratoxin (**1)** for which the exact configuration is known [37]. The results obtained after the optimization of huratoxin (**1**), built from the XRD structure of a parent derivative (12-hydroxydaphnetoxin tribromoacetate) [6], are displayed in **Fig. 6A**, after identification of nine significantly populated conformers. The computed ECD spectra showed similar shape, and the weighted ECD obtained through Boltzmann averaging (**Fig. 6B**) was found to nicely fit the experimental spectrum. As can be seen, the general experimental trends were well reproduced with one positive maxima at 248 nm and a strong negative band around 230 nm.

We therefore computed the ECD spectra of the four huratoxin derivatives (**2-5**) following the same computational protocol and starting from the optimized conformations of huratoxin **1**. In each case, the individual ECD spectra obtained for the various conformers (not shown) were very similar, as observed above for huratoxin. Hence, only the weighted spectra are displayed in **Fig. 6C-F**, where they are overlaid with the experimental ones. The general shapes of the theoretical ECD nicely fit the measured spectra, and the positions of the positive and negative bands were properly estimated, within a ± 0.2 eV range. These results therefore confirmed that the huratoxin derivatives studied herein present the same configuration as huratoxin itself. Note that these results were consistent with previously published ECD spectra for compound **3** [5].

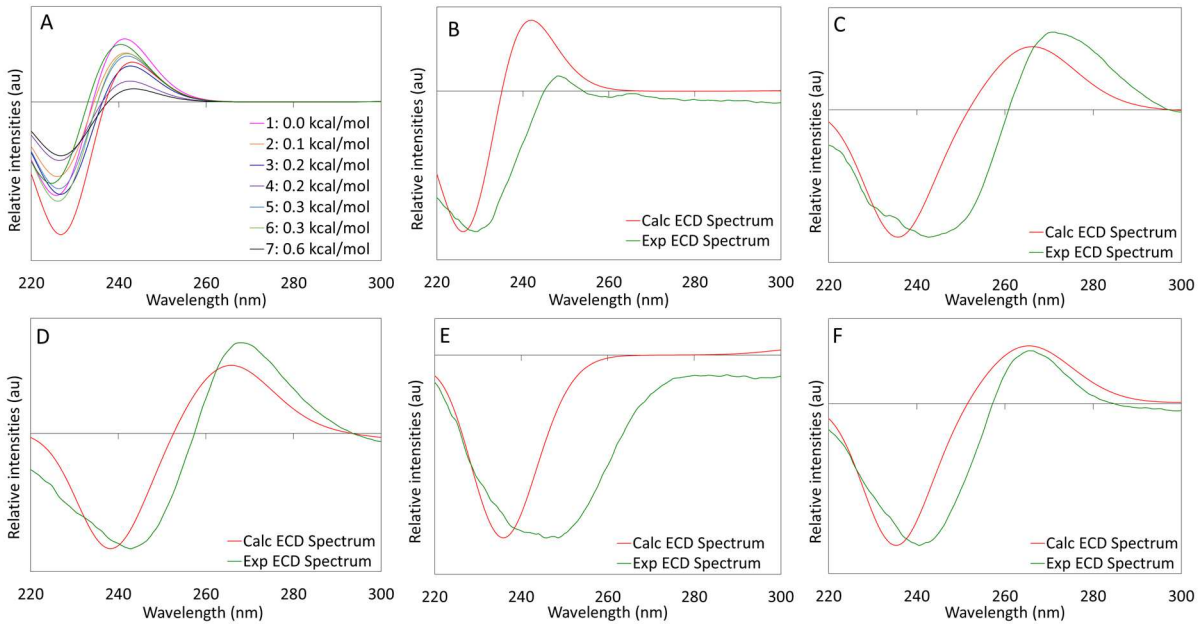

Figure 6. (**A**) Computed ECD spectrum of identified conformers of huratoxin **1.** The relative Gibbs energies are also given. (**B**) Experimental and computed ECD spectra of huratoxin **1**. The computed curve is calculated through Boltzmann averaging of each conformer ECD spectrum. (**C-F**) Computed weighted ECD spectra superimposed to the corresponding experimental curves of prohuratoxin (**C**), stelleralide J (**D**), 2',3'-dihydrohuratoxin (**E**) and 6'-oxohuratoxin (**F**).

3.3. *In vitro activity of isolated mono-esterified daphnanes.*

Due to the minute amounts of the new daphnanes **4** and **5**, only huratoxin (**1**), prohuratoxin (**2**) and stelleralide J (**3**) have been tested according to precedent conditions. TPA, a well-known phorbol ester that exhibited some structural similarities with daphnanes, was used as a positive control since it is known to decrease Caco-2 cell proliferation [42]. As shown in **Fig. 7**, only huratoxin **1** significantly inhibited Caco-2 cell proliferation by 25.33% ± 9.71 at 1 µg/mL, while HT29 and normal IEC6 cells were spared by this treatment, reproducing the selective effect previously observed with the crude extract and the fraction enriched in mono-esterified daphnanes. A similar selective decrease of Caco-2 cells was observed under treatment with TPA (**Fig. 7**). However, prohuratoxin and stelleralide J did not affect cell viability suggesting that the orthoester moiety of daphnane-type diterpenes is essential to their inhibitory activity, as already described in previous reports [4,9,43,44].

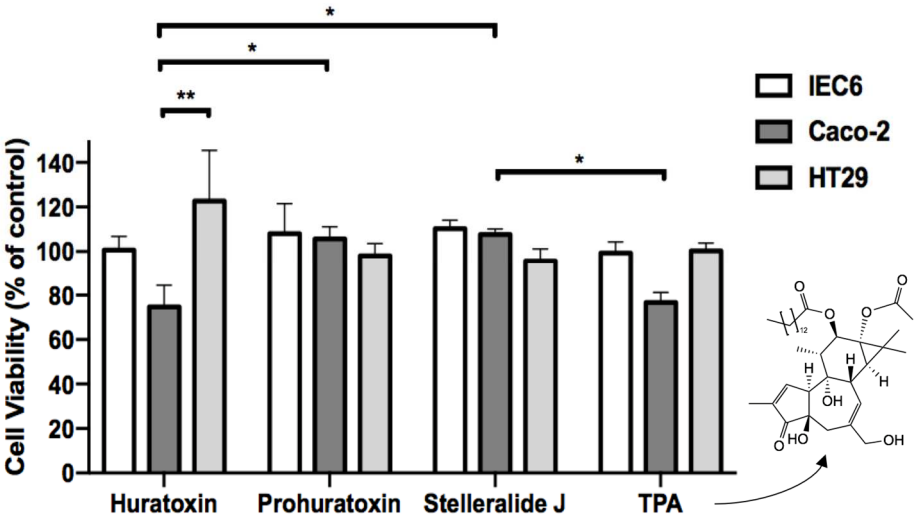

Figure 7. Cytotoxicity of 3 isolated mono-esterified daphnanes from *H. crepitans* latex. IEC6 (normal intestinal cell line), Caco-2 and HT29 (colon cancer cell lines) cells were incubated with 1 µg/mL huratoxin, prohuratoxin or stelleralide J, TPA or DMSO as control. At 48 h, a MTS assay was performed to measure surviving cells. Data are mean ± S.D. from 3 independent experiments. Two-way Anova (Tukey's multiple comparisons test): *p<0.05, **p<0.01.

To further characterize the underlying mechanism of action of huratoxin, the expressions of the proliferation marker Ki67 and the apoptosis marker Caspase 3 were evaluated after treatment. As depicted in **Fig. 8A**, the proliferative marker Ki67 was significantly decreased in Caco-2 cells treated by huratoxin and to a lesser extent by TPA. Labeling of active Caspase 3 was not detected showing that neither huratoxin nor TPA induced cell apoptosis. We concluded that the cytotoxic effect of huratoxin on Caco-2 cells was a cytostatic effect as conjectured above. Moreover, we determined that huratoxin induced a cell growth arrest at the G1 phase (**Fig. 8B**) as previously shown for TPA [45]. Also, huratoxin, and to a lesser extent TPA, induced clustering of Caco-2 cells (**Fig. 8A and 8B**) confirming that there is a potential link between proliferative and morphologic changes.

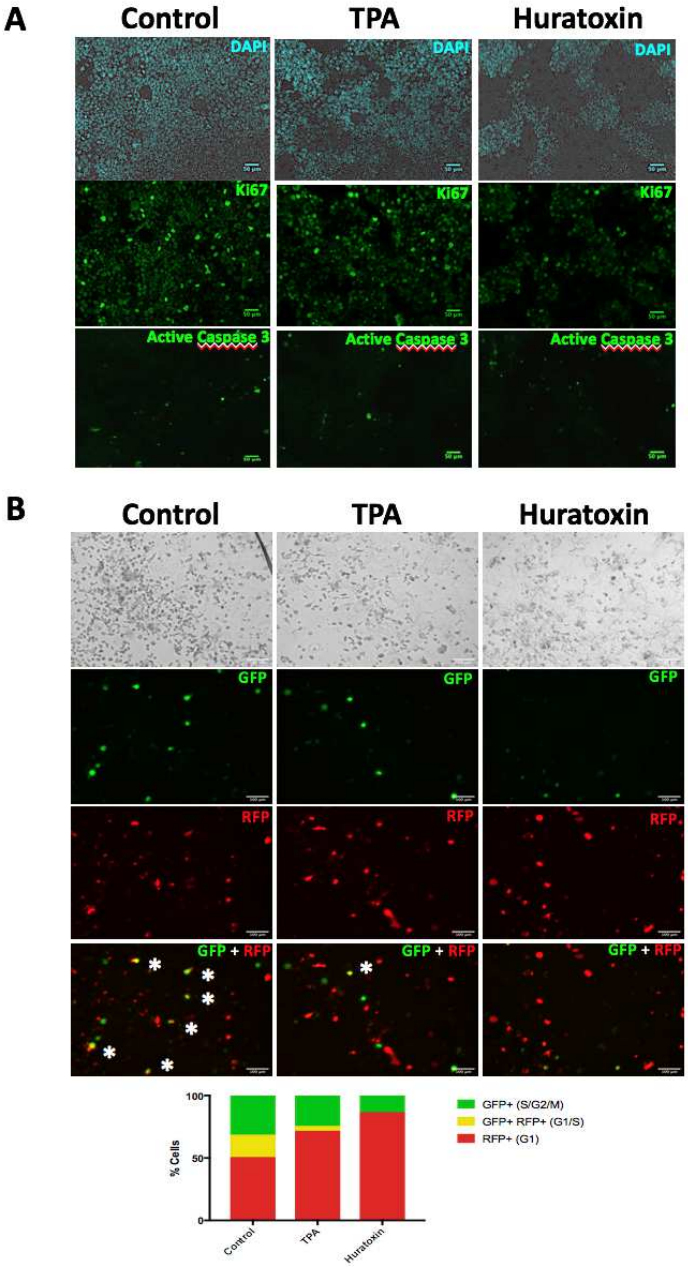

Figure 8. A-Immunolabeling of Ki67 and active caspase 3 in Caco-2 cells treated with huratoxin or TPA. Caco-2 cells were treated with 1 µg/mL of huratoxin or TPA, or DMSO as control for 48 h. Immunolabeling of the proliferative marker Ki67 and apoptosis marker Caspase 3 was performed as described in Experimental section. Nuclei were labeled with DAPI. Bar = 50 µm. Representative of two independent experiments. B- Cell cycle analysis was performed on Caco-2 cells treated as in A using the Premo-FUCCI cell cycle sensor (Experimental section). Representative images of GFP and RFP labeling 96 h after treatment are shown. In merge at the bottom, asterisks indicate cells labeled with both GFP and RFP. A histogram representation shows the percentage of labeled cells corresponding to the phases of cell cycle. Bar = 100 µm. Representative of two independent experiments.

3.4 *Signaling pathways modulated by huratoxin.*

The proliferative and morphologic activities regulated by huratoxin prompted us to investigate signaling pathways known to play a critical role at the crossroad of cell adhesion and proliferation. We reasoned that in Caco-2 cells bringing APC mutation and thus a dysregulated trafficking of β-catenin from the membrane to the nucleus, the signals MAPK, GSK3β, Akt and YAP could be yet modulated by huratoxin. Indeed, as depicted in **Fig. 9**, huratoxin induced inhibition of GSK3β and Akt, two serine threonine kinases playing a major role in colon carcinogenesis.[46] However, unlike huratoxin, TPA did not induce a decrease in those kinase activities but inhibited YAP and activated MAPK (**Fig. 9**), as previously shown in liver cancer [26,47].

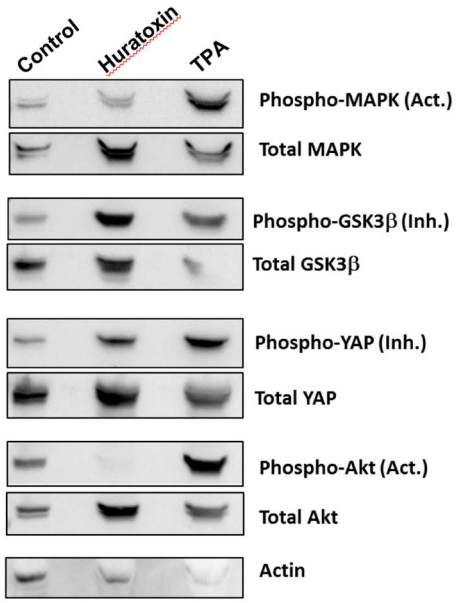

Figure 9. Western blot of MAPK, GSK3β, YAP and Akt in Caco-2 cells treated with huratoxin. Caco-2 cells were treated with 1 μg/mL huratoxin or TPA, or DMSO as control for 48 h. The expression of total proteins and their activated (Act.) or inhibited (Inh.) phosphorylated forms was detected by specific antibodies as described in Experimental section. Actin is shown as a loading control. Representative of two independent experiments.

Clearly the activities of the two structurally similar diterpenes, huratoxin and TPA, are mechanistically different. This could explain the higher cell clustering and decreased Ki67 labeling observed in Caco-2 cells treated by huratoxin as compared to TPA. However, the absence of huratoxin or TPA's impact on HT29 cells (**Fig. 7**) which are characterized by a Raf mutation in addition of APC mutation, suggests that unimpaired Raf/MEK pathway upstream of the proliferative and adhesive signals may be crucial for the cytostatic activity of both diterpenoids [48].

3.5 *Epithelial polarization and differentiation induced by huratoxin.*

We further investigated morphological changes induced by huratoxin. As shown in **Fig. 10A**, Caco-2 cell clustering was already measurable from 24h post-treatment by huratoxin. Interestingly, at 48 h, Caco-2 clusters were organized in relief (around 30 µm high) with cells boarding a central lumen and harboring nucleus in basal position (**Fig. 10B-C**). Actin was concentrated in basal position (**Fig. 10B**), as previously observed in epithelial spheroids formed in the absence of extracellular matrix [49]. By comparison to huratoxin (**Fig. 10B**), TPA was less potent to induce both cell clustering (structures in relief 10 µm high, not shown) and polarization (**Fig. 10D**). These data show that huratoxin induces the formation of structures mimicking the intestinal crypt architecture.

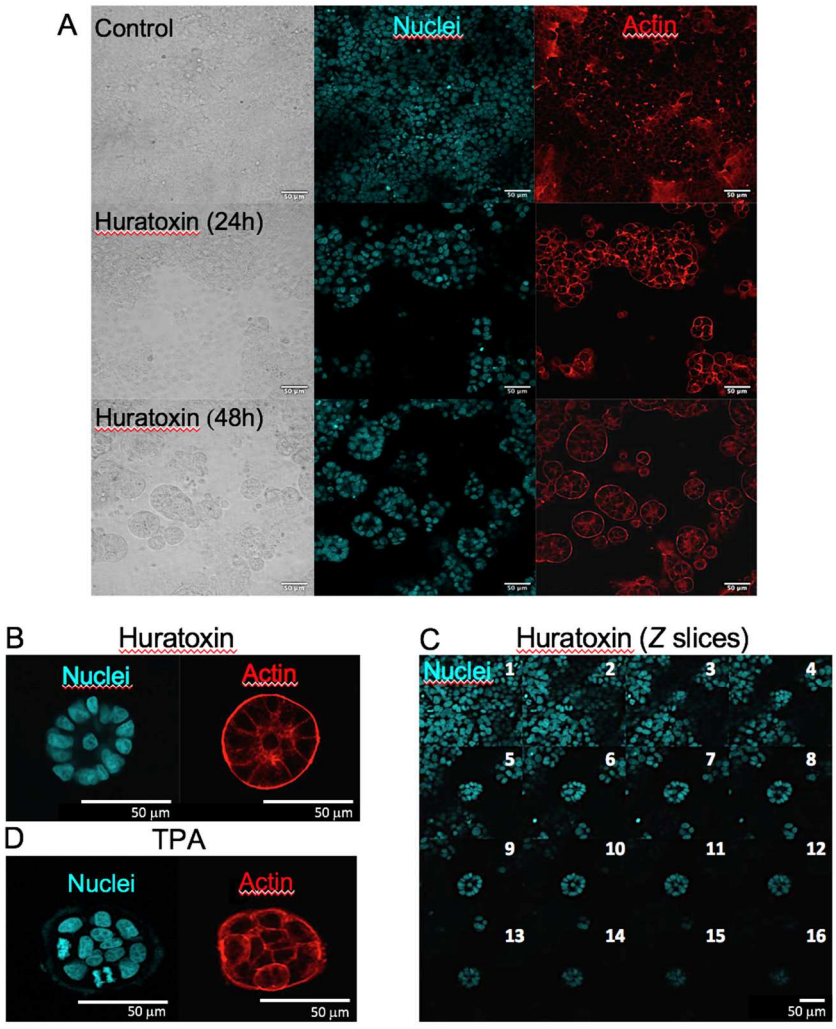

Figure 10. Epithelial polarization upon huratoxin treatment. Caco-2 cells were treated with huratoxin or TPA at 1 µg/mL, or DMSO as control for 48 h. A-D Labeling of nuclei and actin was performed as described in Experimental section and confocal imaging was realized.

Corresponding brightfield images are shown in A. Representative of two experiments. Bar = 50 μm.

Since the change in Caco-2 cells morphology induced by huratoxin suggested the formation of neo-crypts, we wonder if cell differentiation was also triggered. We decided to investigate the gene expression of integrin alpha 2 (ITGA2) and mucin 2 (MUC2) since integrin alpha 2 was shown to regulate the balance between proliferation and differentiation in Caco-2 cells [50] which are deficient in mucous-lineage [51]. As shown in **Fig. 11**, expressions of ITGA2 and MUC2 were increased in huratoxin-treated Caco-2 cells. By comparison to huratoxin, TPA was less potent to induce these changes in gene expression (**Fig. 11**). Therefore, huratoxin induces a cytostatic effect on colon cancer cells accompanied by epithelial morphogenesis.

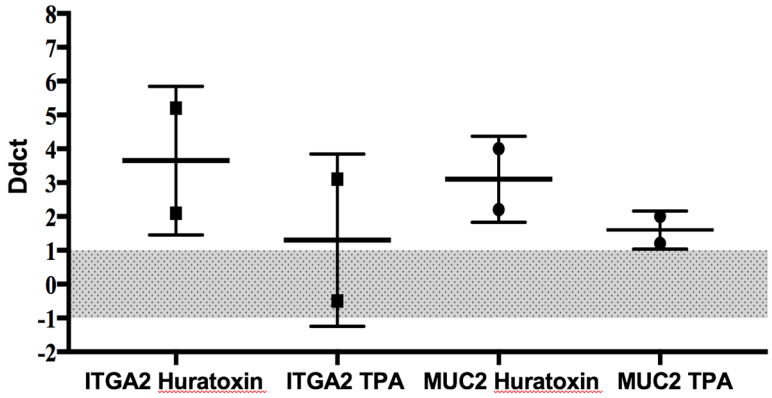

Figure 11. Gene expression of the integrin alpha 2 (ITGA2) and mucin 2 (MUC2) upon huratoxin treatment. Caco-2 cells were treated with huratoxin or TPA at 1 μg/mL, or DMSO as control for 48 h. Quantitative RT-PCR was performed as described in Experimental section. Compared to control, variations between -1 and 1 are considered as not significant (grey zone). Data from two independent experiments are shown.

4. Conclusions

The morphological changes and selective cytotoxic activity against Caco-2 cells induced by an EtOH extract of the latex of *H. crepitans* led to the isolation of two new daphnane-type diterpenoids named 2',3'-dihydrohuratoxin and 6'-oxohuratoxin, along with three known analogs including huratoxin, the main latex component. The biological assessment of the pure three known derivatives highlighted huratoxin as the most interesting compound that was further investigated to decipher its mode of action in comparison with TPA, a commercial phorbol ester-type diterpenoid, known for its cytotoxicity against Caco-2 cells. The two compounds showed a decrease in proliferative marker Ki67 with no effect on caspase 3,

characterizing a cytostatic activity. Concerning signaling pathways, huratoxin inhibited GSK3β and Akt, two kinases playing a major role in colon carcinogenesis, while TPA inhibited YAP and activated MAPK as previously described, thus revealing different cytostatic mechanisms. Finally, huratoxin has been more potent than TPA to induce the expression of two genes implicated in Caco-2 cells differentiation, which might explain the more pronounced morphological changes induced by huratoxin including the formation of neo-crypts. Works are actually in progress to deeply investigate the signaling pathways modulated by huratoxin, particularly those resulting from an activation of PKC isotypes. Finally, our data revealed that, besides their well-known roles as neurotrophic factors, daphnanes diterpenes could also restore the functions of intestinal epithelium.

Funding information

This work was supported by the French Ministry of Higher Education and Research (three years PhD grant) and the European Research Council (ERC- 310973 PIPE to NV).

Competing interests

Declarations of interest: none.

Acknowledgements

We would like to thank Isabelle Fabing (SPCMIB) for help to the purification, Céline Deraeve (LCC) for access to the IR spectrometer, and Pierre Lavedan, Marc Vedrenne and Caroline Toppan from the NMR platform of the Institut de Chimie de Toulouse (ICT) for NMR analyses. The CCIPL (Centre de Calcul des Pays de la Loire) is also greatly acknowledged for providing computational time. Corinne Rolland and Laura Guiraud are acknowledged for their help in experiments of molecular biology.

References

[1] M.M. Gordillo, J.J. Ramirez, R.C. Duran, E.J. Arriaga, R. Garcia, A. Cervantes, R.M. Hernandez, Los géneros de la familia Euphorbiaceae en México, Botanica. 73 (2002) 155–281.

[2] M. Trinel, V. Jullian, A.-C. Le Lamer, I. Mhamdi, K. Mejia, D. Castillo, B.J. Cabanillas, N. Fabre, Profiling of *Hura crepitans* L. latex by ultra-high-performance liquid chromatography/atmospheric pressure chemical ionisation linear ion trap Orbitrap mass spectrometry, Phytochem. Anal. (2018). https://doi.org/10.1002/pca.2776.

[3] W. He, M. Cik, G. Appendino, L. Van Puyvelde, J. Leysen, N. De Kimpe, Daphnane-type diterpene orthoesters and their biological activities, Mini-Reviews in Medicinal Chemistry. 2 (2002) 185–200. https://doi.org/10.2174/1389557024605492.

[4] Y.-X. Jin, L.-L. Shi, D.-P. Zhang, H.-Y. Wei, Y. Si, G.-X. Ma, J. Zhang, A review on daphnane-type diterpenoids and their bioactive studies, Molecules. 24 (2019) 1842. https://doi.org/10.3390/molecules24091842.

[5] M. Yan, Y. Lu, C.-H. Chen, Y. Zhao, K.-H. Lee, D.-F. Chen, Stelleralides D–J and anti-HIV daphnane diterpenes from *Stellera chamaejasme*, J. Nat. Prod. 78 (2015) 2712–2718. https://doi.org/10.1021/acs.jnatprod.5b00660.

[6] J. Coetzer, M.J. Pieterse, The structure of 12-hydroxydaphnetoxin, a poisonous constituent of *Lasiosiphon Burchellii*: an X-ray analysis of 12-hydroxydaphnetoxin tribromoacetate, Acta Cryst. B28 (1972) 620–624.

[7] P.-M. Allard, P. Leyssen, M.-T. Martin, M. Bourjot, V. Dumontet, C. Eydoux, J.-C. Guillemot, B. Canard, C. Poullain, F. Guéritte, M. Litaudon, Antiviral chlorinated daphnane diterpenoid orthoesters from the bark and wood of *Trigonostemon cherrieri*, Phytochemistry. 84 (2012) 160–168. https://doi.org/10.1016/j.phytochem.2012.07.023.

[8] S.-F. Li, Y.-Y. Jiao, Z.-Q. Zhang, J.-B. Chao, J. Jia, X.-L. Shi, L.-W. Zhang, Diterpenes from buds of *Wikstroemia chamaedaphne* showing anti-hepatitis B virus activities, Phytochemistry. 151 (2018) 17–25. https://doi.org/10.1016/j.phytochem.2018.01.021.

[9] S.Z. Huang, X.J. Zhang, X.Y. Li, L.M. Kong, H.Z. Jiang, Q.Y. Ma, Y.Q. Liu, J.M. Hu, Y.T. Zheng, Y. Li, J. Zhou, Y.X. Zhao, Daphnane-type diterpene esters with cytotoxic and anti-HIV-1 activities from *Daphne acutiloba* Rehd., Phytochemistry. 75 (2012) 99–107. https://doi.org/10.1016/j.phytochem.2011.11.013.

[10] L. Zhang, R.-H. Luo, F. Wang, M.-Y. Jiang, Z.-J. Dong, L.-M. Yang, Y.-T. Zheng, J.-K. Liu, Highly functionalized daphnane diterpenoids from *Trigonostemon thyrsoideum*, Org. Lett. 12 (2010) 152–155. https://doi.org/10.1021/ol9025638.

[11] Y.-Y. Cheng, H. Chen, H.-P. He, Y. Zhang, S.-F. Li, G.-H. Tang, L.-L. Guo, W. Yang, F. Zhu, Y.-T. Zheng, S.-L. Li, X.-J. Hao, Anti-HIV active daphnane diterpenoids from *Trigonostemon thyrsoideum*, Phytochemistry. 96 (2013) 360–369. https://doi.org/10.1016/j.phytochem.2013.10.005.

[12] F. Li, Q. Sun, L. Hong, L. Li, Y. Wu, M. Xia, T. Ikejima, Y. Peng, S. Song, Daphnane-type diterpenes with inhibitory activities against human cancer cell lines from *Daphne genkwa*, Bioorg. Med. Chem. Lett. 23 (2013) 2500–2504. https://doi.org/10.1016/j.bmcl.2013.03.025.

[13] K.K. Bang, C.-Y. Yun, C. Lee, Q. Jin, J.W. Lee, S.-H. Jung, D. Lee, M.K. Lee, J.T. Hong, Y. Kim, B.Y. Hwang, Melanogenesis inhibitory daphnane diterpenoids from the flower buds of Daphne genkwa, Bioorg. Med. Chem. Lett. 23 (2013) 3334–3337. https://doi.org/10.1016/j.bmcl.2013.03.096.

[14] B.-Y. Park, B.-S. Min, K.-S. Ahn, O.-K. Kwon, H. Joung, K.-H. Bae, H.-K. Lee, S.-R. Oh, Daphnane diterpene esters isolated from flower buds of *Daphne genkwa* induce apoptosis in human myelocytic HL-60 cells and suppress tumor growth in Lewis lung carcinoma (LLC)-inoculated mouse model, J. Ethnopharmacol. 111 (2007) 496–503. https://doi.org/10.1016/j.jep.2006.12.023.

[15] P.A. Wender, N. Buschmann, N.B. Cardin, L.R. Jones, C. Kan, J.-M. Kee, J.A. Kowalski, K.E. Longcore, Gateway synthesis of daphnane congeners and their protein

kinase C affinities and cell-growth activities, Nat. Chem. 3 (2011) 615–619. https://doi.org/10.1038/nchem.1074.
[16] W. Adolf, E. Hecker, On the active principles of the spurge family, X. Skin irritants, cocarcinogens, and cryptic cocarcinogens from the latex of the manchineel tree, J. Nat. Prod. 47 (1984) 482–496.
[17] W. Dagang, B. Sorg, W. Adolf, E.H. Seip, E. Hecker, Oligo-and macrocyclic diterpenes in thymelaeaceae and euphorbiaceae occurring and utilized in Yunnan (Southwest China) 1. Daphnane type diterpene esters from *Daphne feddei*, Phytotherapy Research. 5 (1991) 163–168.
[18] W. He, M. Cik, L. Van Puyvelde, J. Van Dun, G. Appendino, A. Lesage, I. Van der Lindin, J.E. Leysen, W. Wouters, S.G. Mathenge, F.P. Mudida, N. De Kimpe, Neurotrophic and antileukemic daphnane diterpenoids from *Synaptolepis kirkii*, Bioorganic & Medicinal Chemistry. 10 (2002) 3245–3255. https://doi.org/10.1016/S0968-0896(02)00163-3.
[19] B.-S. Han, K.-S. Kim, Y.J. Kim, H.-Y. Jung, Y.-M. Kang, K.-S. Lee, M.-J. Sohn, C.-H. Kim, K.-S. Kim, W.-G. Kim, Daphnane diterpenes from *Daphne genkwa* activate Nurr1 and have a neuroprotective effect in an animal model of parkinson's disease, J. Nat. Prod. 79 (2016) 1604–1609. https://doi.org/10.1021/acs.jnatprod.6b00110.
[20] C. Antal, A. Hudson, E. Kang, C. Zanca, C. Wirth, N. Stephenson, E. Trotter, L. Gallegos, C. Miller, F. Furnari, T. Hunter, J. Brognard, A. Newton, Cancer-associated Protein Kinase C mutations reveal kinases role as tumor suppressor, Cell. 160 (2015) 489–502. https://doi.org/10.1016/j.cell.2015.01.001.
[21] World Health Organization, Cancer today, (n.d.). http://gco.iarc.fr/today/home (accessed September 18, 2018).
[22] A. Vincent, A. Ouelkdite-Oumouchal, M. Souidi, J. Leclerc, B. Neve, I.V. Seuningen, Colon cancer stemness as a reversible epigenetic state: Implications for anticancer therapies, World J Stem Cells. 11 (2019) 920–936. https://doi.org/10.4252/wjsc.v11.i11.920.
[23] H. Gehart, H. Clevers, Tales from the crypt: new insights into intestinal stem cells, Nat Rev Gastroenterol Hepatol. (2019) 19–34.
[24] A. Farhadi, A. Keshavarzian, Z. Ranjbaran, J.Z. Fields, A. Banan, The role of Protein Kinase C isoforms in modulating injury and repair of the intestinal barrier, J. Pharmacol. Exp. Ther. 316 (2006) 1–7. https://doi.org/10.1124/jpet.105.085449.
[25] E.M. Schmidt, S. Lamprecht, C. Blaj, C. Schaaf, S. Krebs, H. Blum, H. Hermeking, A. Jung, T. Kirchner, D. Horst, Targeting tumor cell plasticity by combined inhibition of NOTCH and MAPK signaling in colon cancer, J. Exp. Med. 215 (2018) 1693–1708. https://doi.org/10.1084/jem.20171455.
[26] G. Zhu, Y. Chen, X. Zhang, Q. Wu, Y. Zhao, Y. Chen, F. Sun, Y. Qiao, J. Wang, 12-O-Tetradecanoylphorbol-13-acetate (TPA) is anti-tumorigenic in liver cancer cells via inhibiting YAP through AMOT, Scientific Reports. 7 (2017) 44940. https://doi.org/10.1038/srep44940.
[27] S. Dutta, S. Mahalanobish, S. Saha, S. Ghosh, P.C. Sil, Natural products: an upcoming therapeutic approach to cancer, Food Chem. Toxicol. 128 (2019) 240–255. https://doi.org/10.1016/j.fct.2019.04.012.
[28] M.J. Frisch, G.W. Trucks, H.B. Schlegel, G.E. Scuseria, M.A. Robb, J.R. Cheeseman, G. Scalmani, V. Barone, G.A. Petersson, H. Nakatsuji, X. Li, M. Caricato, A.V. Marenich, J. Bloino, B.G. Janesko, R. Gomperts, B. Mennucci, H.P. Hratchian, J.V. Ortiz, A.F. Izmaylov, J.L. Sonnenberg, D. Williams-Young, F. Ding, F. Lipparini, F. Egidi, J. Goings, B. Peng, A. Petrone, T. Henderson, D. Ranasinghe, V.G. Zakrzewski, J. Gao, N. Rega, G. Zheng, W. Liang, M. Hada, M. Ehara, K. Toyota, R. Fukufa, J. Hasegawa, M.

Ishida, T. Nakajima, Y. Honda, O. Kitao, H. Nakai, T. Vreven, K. Throssell, J.A. Montgomery, J.E. Peralta, F. Ogliaro, M.J. Bearpark, J.J. Heyd, E.N. Brothers, K.N. Kudin, V.N. Staroverov, T.A. Keith, R. Kobayashi, J. Normand, K. Raghavachari, A.P. Rendell, J.C. Burant, S.S. Iyengar, J. Tomasi, M. Cossi, J.M. Millam, M. Klene, C. Adamo, R. Cammi, J.W. Ochterski, R.L. Martin, K. Morokuma, O. Farkas, J.B. Foresman, D.J. Fox, Gaussian 16, Revision A.03. Gaussian, Inc. Wallingford CT., (2016).

[29] A.D. Becke, Density-functional thermochemistry. III. The role of exact exchange, J. Chem. Phys. 98 (1993) 5648–5652.

[30] B. Tomasi, B. Mennucci, R. Cammi, Quantum mechanical continuum solvation models, Chem. Rev. 105 (2005) 2999–3093.

[31] D. Jacquemin, C. Adamo, Computational molecular electronic spectroscopy with TD-DFT, Top. Curr. Chem. 368 (2016) 347–375.

[32] S.M. Kupchan, Y. Shizuri, W.C. Sumner, H.R. Haynes, A.P. Leighton, B.R. Sickles, The isolation and structural elucidation of new potent antileukemic diterpenoid esters from *Gnidia* species, J. Org. Chem. 41 (1976) 3850–3853. https://doi.org/10.1021/jo00886a016.

[33] F. Abe, Y. Iwase, T. Yamauchi, K. Kinjo, S. Yaga, M. Ishii, M. Iwahana, Minor daphnane-type diterpenoids from *Wikstroemia retusa*, Phytochemistry. 47 (1998) 833–837. https://doi.org/10.1016/S0031-9422(97)00529-3.

[34] M. Garcia-Barros, N. Coant, T. Kawamori, M. Wada, A.J. Snider, J.-P. Truman, B.X. Wu, H. Furuya, C.J. Clarke, A.B. Bialkowska, A. Ghaleb, V.W. Yang, L.M. Obeid, Y.A. Hannun, Role of neutral ceramidase in colon cancer, The FASEB Journal. 30 (2016) 4159–4171.

[35] V. Thamilselvan, W. Li, B.E. Sumpio, M.D. Basson, Sphingosine-1-phosphate stimulates human Caco-2 intestinal epithelial proliferation via p38 activation and activates ERK by an independent mechanism, In Vitro Cell. Dev. Biol. - Animal. 38 (2002) 246–253.

[36] T. Chen, Z. Huang, R. Liu, J. Yang, P.B. Hylemon, H. Zhou, Sphingosine-1 phosphate promotes intestinal epithelial cell proliferation via S1PR2, Front Biosci (Landmark Ed). 22 (2017) 596–608. https://doi.org/10.2741/4505.

[37] K. Sakata, K. Kawazu, T. Mitsui, N. Masaki, Structure and stereochemistry of huratoxin, a piscicidal constituent of *Hura crepitans*, Tetrahedron Lett. 12 (1971) 1141–1144.

[38] S.D. Jolad, J.J. Hoffmann, B.N. Timmermann, K.H. Schram, J.R. Cole, R.B. Bates, R.E. Klenck, M.S. Tempesta, Daphnane diterpenes from *Wikstroemia monticola*: wikstrotoxins A-D, huratoxin, and excoecariatoxin, J. Nat. Prod. 46 (1983) 675–680. https://doi.org/10.1021/np50029a015.

[39] L. Barbieri, A. Falasca, C. Franceschi, F. Licastro, C.A. Rossi, F. Stirpe, Purification and properties of two lectins from the latex of the euphorbiaceous plants *Hura crepitans* L. (sand-box tree) and *Euphorbia characias* L. (Mediterranean spurge)., Biochem. J. 215 (1983) 433.

[40] H.-B. Wang, L.-P. Liu, X.-Y. Wang, 13C-NMR data of daphnane diterpenoids, Magn. Reson. Chem. 51 (2013) 580–592. https://doi.org/10.1002/mrc.3978.

[41] F.D. Gunstone, M.R. Pollard, C.M. Scrimgeour, H.S. Vedanayagam, Fatty acids. Part 50. 13C nuclear magnetic resonance studies of olefinic fatty acids and esters, Chemistry and Physics of Lipids. 18 (1977) 115–129. https://doi.org/10.1016/0009-3084(77)90031-7.

[42] S.R. Cerda, R. Mustafi, H. Little, G. Cohen, S. Khare, C. Moore, P. Majumder, M. Bissonnette, Protein kinase C delta inhibits Caco-2 cell proliferation by selective

changes in cell cycle and cell death regulators, Oncogene. 25 (2006) 3123–3138. https://doi.org/10.1038/sj.onc.1209360.
[43] E. Stanoeva, W. He, N. De Kimpe, Natural and synthetic cage compounds incorporating the 2,9,10-trioxatricyclo[4.3.1.03,8]decane type moiety, Bioorg. Med. Chem. 13 (2005) 17–28. https://doi.org/10.1016/j.bmc.2004.07.070.
[44] S.-G. Liao, H.-D. Chen, J.-M. Yue, Plant orthoesters, Chem. Rev. 109 (2009) 1092–1140. https://doi.org/10.1021/cr0782832.
[45] S. Dupasquier, P. Blache, L. Picque Lasorsa, H. Zhao, J.-D. Abraham, J.J. Haigh, M. Ychou, C. Prévostel, Modulating PKCα activity to target Wnt/β-catenin signaling in colon cancer, Cancers (Basel). 11 (2019). https://doi.org/10.3390/cancers11050693.
[46] S. Afrin, F. Giampieri, M. Gasparrini, T.Y. Forbes-Hernández, D. Cianciosi, P. Reboredo-Rodriguez, A. Amici, J.L. Quiles, M. Battino, The inhibitory effect of Manuka honey on human colon cancer HCT-116 and LoVo cell growth. Part 1: the suppression of cell proliferation, promotion of apoptosis and arrest of the cell cycle, Food Funct. 9 (2018) 2145–2157. https://doi.org/10.1039/C8FO00164B.
[47] W.-S. Wu, The signaling mechanism of ROS in tumor progression, Cancer Metastasis Rev. 25 (2006) 695–705. https://doi.org/10.1007/s10555-006-9037-8.
[48] L.A. Barbosa, L. Goto-Silva, P.A. Redondo, S. Oliveira, G. Montesano, W. de Souza, J.A. Morgado-Díaz, TPA-induced signal transduction: a link between PKC and EGFR signaling modulates the assembly of intercellular junctions in Caco-2 cells, Cell Tissue Res. 312 (2003) 319–331. https://doi.org/10.1007/s00441-003-0727-z.
[49] J.Y. Co, M. Margalef-Català, X. Li, A.T. Mah, C.J. Kuo, D.M. Monack, M.R. Amieva, Controlling epithelial polarity: a human enteroid model for host-pathogen interactions, Cell Reports. 26 (2019) 2509-2520.e4. https://doi.org/10.1016/j.celrep.2019.01.108.
[50] S.C. Kirkland, H. Ying, Alpha2beta1 integrin regulates lineage commitment in multipotent human colorectal cancer cells, J. Biol. Chem. 283 (2008) 27612–27619. https://doi.org/10.1074/jbc.M802932200.
[51] Y. Li, E. Arranz, A. Guri, M. Corredig, Mucus interactions with liposomes encapsulating bioactives: interfacial tensiometry and cellular uptake on Caco-2 and cocultures of Caco-2/HT29-MTX, Food Research International. 92 (2017) 128–137. https://doi.org/10.1016/j.foodres.2016.12.010.

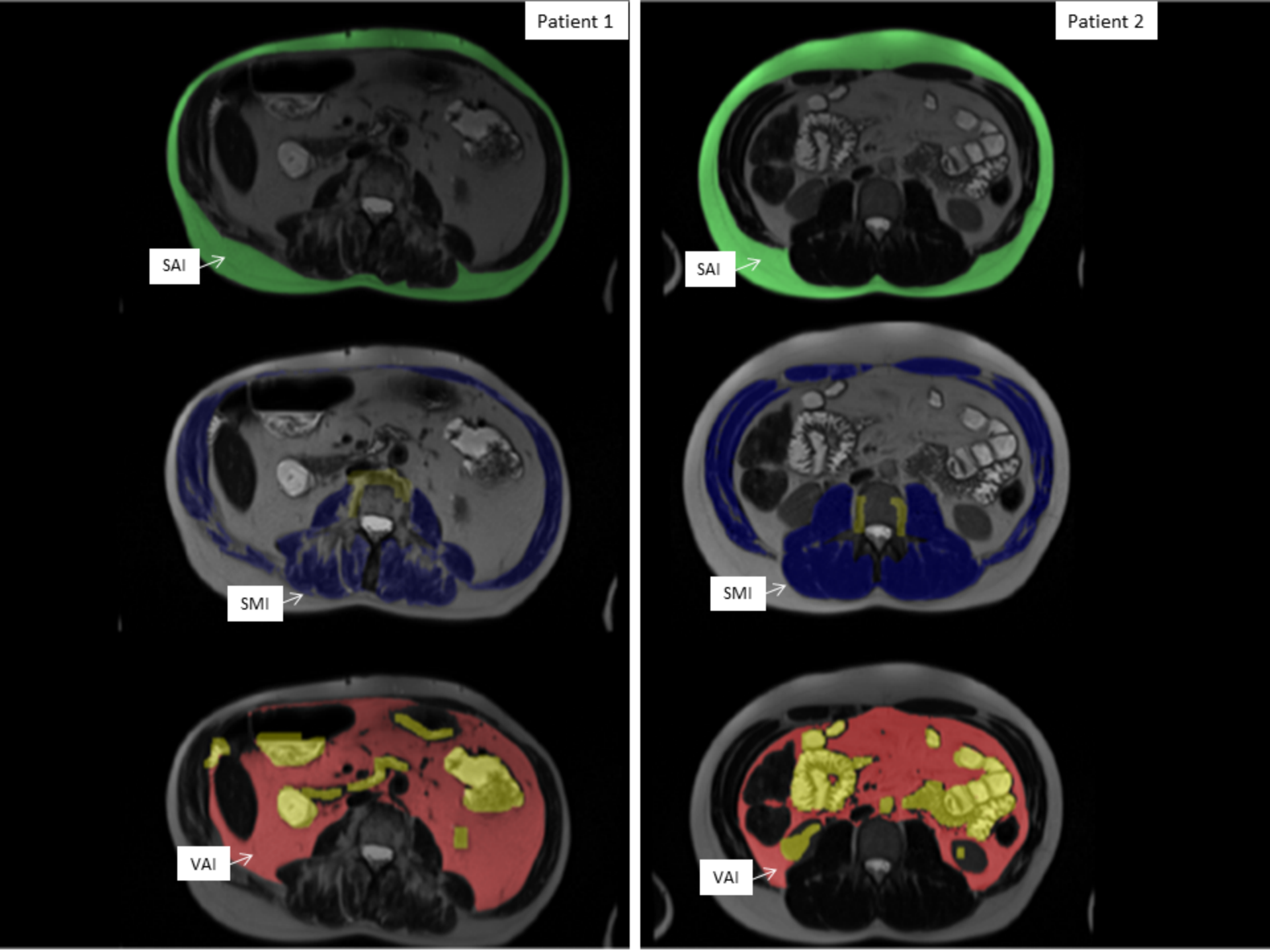
Patient 1
SAI
SMI
VAI
Patient 2
SAI
SMI
VAI

Table 1: Cohort demographic's between groups.

		TOTAL (n=132)	Inactive disease (n = 74)	Active disease (n = 58)	n	p	
DURATION		10.4 (4.69)	9.95 (±4.89)	10.9 (±4.41)	132	0.25	
AGE		36.9 (12.0)	36.6 (±12.9)	37.4 (±10.8)	132	0.72	
GENDER	F	75 (57%)	44 (59%)	31 (53%)	75	0.61	
	M	57 (43%)	30 (41%)	27 (47%)	57	-	
Montreal classification							
AGE AT DIAGNOSIS	A2	104 (79%)	52 (70%)	52 (90%)	111	**-**	
	A3	19 (14.1%)	17 (23%)	2 (3.4%)	12	**<0.01**	
	A1	9 (6.8%)	5 (6.8%)	4 (6.9%)	9	-	
LOCATION	L3	67 (51%)	41 (55%)	26 (45%)	67	0.53	
	L1	29 (22%)	14 (19%)	15 (26%)	29	-	
	L2	23 (17%)	11 (15%)	12 (21%)	23	-	
	L4	13 (9.8%)	8 (11%)	5 (8.6%)	13	-	
BEHAVIOUR	B1	39 (30%)	30 (41%)	9 (16%)	39	**<0.001**	
	B2	33 (25%)	15 (26%)	15 (26%)	33	-	
	B3	25 (19%)	8 (11%)	18 (24%)	25	-	
	B1p	14 (11%)	11 (15%)	3 (5.2%)	14	-	
	b2p	12 (9.1%)	5 (6.8%)	7 (12%)	12	-	
	B3p	9 (6.8%)	2 (2.7%)	7 (12%)	9	-	
PERIANAL SURGERY	YES	30 (23%)	13 (18%)	17 (29%)	30	0.16	
BOWEL RESECTION	YES	51 (39%)	27 (36 %)	24 (41%)	51	0.69	
TABAGISM	YES	26 (20%)	9 (12%)	17 (29%)	26	**0.025**	
ACTUAL THERAPY	BIOTHERAPY IMMUNOMODULATOR	68 (52%)	35 (47%)	33 (57%)	68	0.36	
	OTHER	64 (48%)	39 (53%)	25 (43 %)	64	-	

Table 2 : Intra-observer correlation for MRI measurements of body composition

	INTERCEPT (IC 95%)	SLOPE (IC 95%)	Spearman coefficient	P
SMI	0,3648 (-1,8421 to 2,2580)	1,0049 (0,9677 to 1,0526)	0,9729	<0,0001
VAI	0,4497 (-2,8679to 3,0097)	1,0582 (0,9734 to 1,1602)	0,9519	<0,0001
SAI	0,0462 (-1,1852to 1,0763)	1,0125(0,9939 to 1,0300)	0,9949	<0,0001

Table 3 : Body composition parameters (means and between gender)

BODY COMPOSITION	TOTAL	p
BMI	22.8 (5.13)	-
UNDERWEIGHT	29 (22%)	-
NORMALWEIGHT	73(55%)	
OVERWEIGHT	30 (23%)	-
SMI	47.0 (12.9)	-
SARCOPENIA*	53 (40%)	-
VAI	35.9 (23.0)	-
SAI	61.0 (42.6)	-
VA/TA(i)	39.1 (14.6)	-
BMI (M vs F)	0.581 [-1.13; 2.32]*	0.52
SMI (M vs F)	11.6 [7.51; 15.6]*	**<0.001**
SARCOPENIA (M vs F)	1.31 [0.649; 2.65]*	0.45
SAI (M vs F)	-24.9 [-39.2; -10.7]*	**<0.001**
VAI (M vs F)	20.4 [13.2; 27.6]*	**<0.001**
VA/TA(i) (M vs F)	22.6 [19.4; 25.9]*	**<0.001**

SAI: subcutaneous adiposity index, VAI: visceral adiposity index, SMI: skeletal muscle index

M vs F : male versus female

* confidence interval

Table 4 : Matrix of correlation between body composition parameters and gender (Pearson coefficients)

	BMI	SMI	VAI	SAI
BMI	1	F : 0,49 M : 0,47	F : 0,69 M : 0,86	F : 0,89 M : 0,76
SMI	F : 0,49 M : 0,47	1	F : 0,30 M : 0,4	F : 0,45 M : 0,47
VAI	F : 0,69 M : 0,86	F : 0,3 M : 0,4	1	F : 0,70 M : 0,75
SAI	F : 0,89 M : 0,76	F : 0,45 M : 0,47	F : 0,70 M : 0,75	1

SAI: subcutaneous adiposity index, VAI: visceral adiposity index, SMI: skeletal muscle index

Table 5 : univariate and multivariate analysis explaining body composition parameters by group

Body composition	Inactive to low disease	Active to severe disease	Difference (univariate)	P	Difference (multivariate)*	P
BMI (ALL)	23.6 (±5.27)	21.7 (±4.78))	**-1.86 [-3.62; -0.102]**	**0.038**	**-1.88 [-3.69; -0.0768]**	**0.041**
F	23.3 (±5.58)	21.3 (±4.83)	-1.99 [-4.46; 0.479]	0.11	-	
M	23.9 (±4.86)	22.1 (±4.77)	-1.79 [-4.35; 0.776]	0.17	-	
SMI (ALL)	48.9 (±13.2)	44.5 (±12.2)	**-4.47 [-8.90; -0.0320]**	**0.048**	**-4.90 [-9.36; -0.431]**	**0.032**
F	43.9 (±11.6)	39.3 (±10.1)	-4.61 [-9.75; 0.528]	0.078	-	
M	56.3 (±12.1)	50.4 (±11.8)	-5.91 [-12.3; 0.444]	0.068	-	
SARCOPENIA (ALL)	24 (32%)	29(50%)	**OR : 2.08 [1.03; 4.27]**	**0.042**	**2.07 [1.02; 4.27]**	**0.046**
F	14 (32%)	15(48%)	OR : 1.76 [0.683; 4.62]	0.24	-	
M	11 (37%)	16 (59%)	OR : 2.50 [0.867; 7.52]	0.094	-	
VAI (ALL)	34.2 (±23.2)	38.0 (±22.8)	**3.82 [-3.53; 11.9]**	0.36	**3.91 [-3.50; 11.9]**	0.34
F	26.0 (±16.2)	28.6 (±16.1)	2.63 [-4.94; 10.2]	0.49	-	
M	46.2 (±26.7)	48.8 (±24.8)	2.58 [-10.1; 17.1]	0.73	-	
SAI (ALL)	67.5 (±46.8)	52.7 (±35.2)	**-14.8 [-29.4; -0.184]**	**0.047**	**-14.7 [-29.8; 0.258]**	**0.054**
F	77.8 (±51.3)	63.3 (±39.2)	14.5 [-36.3; 7.39]	0.19	-	
M	52.5 (±34.7)	40.6 (±25.6)	11.9 [-28.3; 4.44]	0.15	-	
VA/TA(i) (ALL)	34.6 (±12.7)	44.9 (±14.9)	**10.3 [5.56; 15.1]**	**<0.001**	**9.40 [4.72; 14.1]**	**<0.001**
F	25.9 (±7.09)	34.3 (±9.87)	8.45 [4.55; 12.4]	**<0.001**	-	
M	47.4 (±6.78)	57.1 (±9.36)	9.69 [5.38; 14.0]	**<0.001**	-	

* the multivariate analysis adjusted of confounding factors was only possible for the overall effect because in the gender-related subgroups the homoscedasticity condition was not respected.

SAI: subcutaneous adiposity index, VAI: visceral adiposity index, SMI: skeletal muscle index